Assessment of stochastic weather forecast of precipitation near European cities, based on analogs of circulation

Meriem Krouma [1,2], Pascal Yiou [2], Céline Déandreis [1], and Soulivanh Thao [2]

[1]ARIA Technologies, 8 Rue de la Ferme, 92100 Boulogne-Billancourt, France
[2]Laboratoire des Sciences du Climat et de l'Environnement, UMR 8212 CEA-CNRS-UVSQ, IPSL & Université Paris-Saclay, 91191 Gif-sur-Yvette, France

Correspondence: Meriem Krouma (meriem.krouma@lsce.ipsl.fr)

Abstract.

In this study, we ~~aim to~~ assess the skill of a stochastic weather generator (SWG) to forecast precipitation in several cities ~~of~~ in Western Europe. The SWG is based on a random sampling of analogs of the geopotential height at 500 hPa (Z500). The SWG is evaluated for two reanalyses (NCEP and ERA5). We simulate 100-member ensemble forecasts on a daily time increment. We evaluate the performance of SWG with forecast skill scores and we compare it to ECMWF forecasts.

Results show significant positive skill score (continuous rank probability skill score and correlation) ~~comparing~~ compared to persistence and climatology forecasts for lead times of 5 and 10 days for different areas in Europe. We find that the low predictability episodes of our model ~~is~~ are related to specific weather regimes, depending on the European region. Comparing the SWG forecasts to ECMWF forecasts, we find that the SWG shows a good performance for 5 days. This performance varies from one region to another. This paper is a proof of concept for a stochastic regional ensemble precipitation forecast. Its parameters (e.g. region for analogs) must be tuned for each region in order to optimize its performance.

1 Introduction

Ensemble weather forecasts were designed to overcome the issues of meteorological chaos, from which small uncertainties in initial conditions can lead to a wide range of possible trajectories (Sivillo et al., 1997; Palmer, 2000). Hence, from a sufficiently large ensemble of initial conditions, it is in principle possible to sample the probability distribution of future states of the system.

Forecasts issued by meteorological centers are obtained by computing several simulations with perturbed initial conditions, in order to sample uncertainties. Those experiments are rather costly in terms of computing resources and are generally limited to a few tens of members (Hersbach et al., 2020; Toth and Kalnay, 1997), which can hinder a proper estimate of probability distributions of trajectories. Moreover, obtaining information at local spatial scales can be difficult because the horizontal resolution of the atmospheric models is around 18 km, e.g. for the European Centre for Medium-Range Weather Forecasts (ECMWF) ensemble forecast system.

From a mathematical point of view, computing the probability distribution of the trajectories of a (deterministic) system makes the underlying assumption that the system behaves like a stochastic process, for which statistical properties are defined naturally (Ruelle, 1979; Eckmann and Ruelle, 1985). This has justified the development of stochastic weather generators

(SWG), which are stochastic processes that emulate the behavior of key climate variables (Ailliot et al., 2015). The advantages of stochastic models are a relative simplicity of implementation and a low computing cost. The challenge of their development is to verify that the behavior of the simulations ~~are~~ is realistic, according to well-defined criteria (van den Dool, 2007; Jolliffe and Stephenson, 2011).

The first stochastic weather generators were devised to simulate rainfall occurrence ~~by Gabriel and Neumann (1962)~~ (Gabriel and Neuma and to simulate rainfall amounts ~~by Todorovic and Woolhiser (1975)~~(Todorovic and Woolhiser, 1975). SWGs were developed and used to estimate the probability distributions of climate variables such as temperature, solar radiation, and precipitation through extensive simulations (Richardson, 1981).

Stochastic weather generators can be useful complements to atmospheric circulation models, in order to simulate large ensembles of local variables, as they can be calibrated for small spatial scales ~~comparing~~ compared to numerical models (Ailliot et al., 2015). This explains their wide applications in impact studies.

A successful simulation with a SWG relies on the choice of inputs. ~~One of them consists in the use of the atmospheric circulation as~~ The atmospheric circulation can be chosen a predictor for other local variables. The (loose) rationale for this choice is that the circulation is modeled by prognostic equations (Peixoto and Oort, 1992), that drive the other physical variables. Therefore the primitive equations of the atmosphere (Peixoto and Oort, 1992, Chap. 3) suggest that reproducing temporal variability on daily time scales requires considering circulation variables. The influence of large-scale circulation on local climate variables has been proven in previous studies such as the influence of atmospheric circulation on the Mediterranean Basin (Mastrantonas et al., 2021) and Greece's precipitation (Xoplaki et al., 2000; Türkes et al., 2002). Similar influences have been found on precipitation and temperature over the North Atlantic region (Jézéquel et al., 2018b).

Analogs of circulation were initially designed to provide "model-free" forecasts, by assuming that similar situations in atmospheric circulation may lead to similar local weather conditions (Lorenz, 1969). The potential to simulate large ensembles of ~~forecasts~~ forecast temperature with circulation analogs was explored by Yiou and Déandréis (2019), by considering random resamplings of K best analogs (rather than only considering the best analog). This has ~~lead~~ led to the development of a SWG in "predictive" mode, which uses updates of reanalysis datasets ~~(Kistler et al., 2001)~~ as input.

Alternative systems of analogs to forecast precipitation have been proposed by Atencia and Zawadzki (2014). Those systems are based on analogs of precipitation itself. Such systems are very efficient for nowcasting, i.e. forecasting precipitation within the next few hours. Considering the atmospheric circulation analogs allows ~~to focus~~ focusing on longer time scales.

Yiou and Déandréis (2019) evaluated ensemble forecasts of the analog SWG for temperature and the NAO index with classical probability scores against climatology and persistence. Reasonable scores were obtained up to 20 days. Through this study, we aim to assess the skill of this SWG to forecast precipitation in different areas of Europe and for different lead times. The previous study on this ~~forecast~~ forecasting tool was a proof of concept for temperature. In this study, we will adapt the parameters of the analog SWG to optimize the simulation of European precipitations. We then analyse the performance of this SWG for lead times of 5 to 20 days, with the forecast skill scores used by Yiou and Déandréis (2019).

We will evaluate the seasonal dependence of the forecast skills of precipitation and the conditional dependence ~~to~~ on weather regimes. Finally, comparisons with ~~medium range~~ medium-range precipitation forecasts from the ECMWF will be performed.

The paper is divided as follows: Section 2 is dedicated to ~~describe~~ describing the data used for the experiments. Section 3 explains the methodology (analogs, stochastic weather generator and forecast skill scores). Section 4 details the experimental ~~set up~~ setup and justifies the ~~choices~~ choice of parameters that we made for the forecast parameters. Section 5 details the results of simulations and the evaluation of the ensemble forecast. Section 6 contains the main conclusions of the analyses.

2 Data

Daily precipitation data were obtained from the European Climate Assessment and Data (ECAD) project (Klein Tank et al., 2002) for four locations in western Europe (Berlin, Madrid, Orly, Toulouse), which are subject to contrasted meteorological influences (Figure 1). ECAD provides station data ~~,~~ that are available at a daily time step from 1948 to 2019. The choice of those stations was based on the availability of a large and common period of observations with a low rate of missing data (less than 10%). For verification ~~issues~~purposes, we used also the E-Obs data (Haylock et al., 2008), which are a daily gridded data available from 1979 to the present with a horizontal resolution of 0.25° × 0.25°. E-Obs data are spatial interpolations of ECAD data.

We recovered the geopotential height at 500 hPa (Z500) and sea level pressure (SLP) fields from the reanalysis of the National Centers for Environmental Prediction (NCEP: Kistler et al. (2001)) with a spatial resolution of 2.5° × 2.5° from 1 January 1948 to 31 December 2019.

We also used the atmospheric reanalysis (version 5) of the European Centre for Medium-Range Weather Forecasts (ECMWF) (ERA5; Hersbach et al. (2020)). ERA5 data are available from 1950 to the present with a horizontal resolution of 0.25° × 0.25°. ~~There are fundamental differences between the two reanalyses, in the~~ The two reanalysis have fundamental differences in terms of atmospheric models, assimilated data ~~, and assimilation schemes~~and assimilation scheme.

We considered the daily averages of Z500 from NCEP and ERA5, over the region covering 30°W – 20°E and 40°– 60°N, to compute circulation analogs. Daily averages of SLP were used over the region covering 80°W – 20°E and 30° – 70°N to define weather regimes.

In order to assess the predictive skill of our precipitation forecast model, a comparison with another forecast was made. ~~There are many available datasets that~~ Many available datasets can be used for deriving this information. We considered the ECMWF ensemble forecast dataset system 5 (Vitart et al., 2017). It is a daily gridded dataset interpolated over Europe ~~to provide information covering the all the domain~~that provides information covering all the domains. Data are available through the Copernicus Climate Data Store~~including~~ . They include forecasts created in real-time (since 2017) and hindcast forecasts from 1993 to 2019 (Vitart et al., 2017). The data are provided at an hourly time step with a horizontal resolution of 0.25° × 0.25°. We considered the grid points that include Berlin, Orly, Toulouse and Madrid, which were identified in the ECAD database.

3 Methodology

3.1 Analogs

The first step is to build a database of analogs of the atmospheric circulation. We outline the procedure of Yiou and Déandréis (2019), summarized in Figure 1a. For a given day t, we determine the similarity of Z500 for all days t' that are within 30 calendar days of t but in a different year from t. The similarity is quantified by a Euclidean distance (or root mean square error) between the daily Z500 maps. Other types of ~~distances~~ similarity measures are possible (Blanchet et al., 2018), but the expected impact on the results is often marginal (Toth, 1991). We believe that the simplicity of the ~~a~~ Euclidean distance makes it more robust to changes in horizontal resolution (e.g. from NCEP to ERA5), compared to more sophisticated distances that include local spatial gradients, which would require adjustments and additional tuning. This choice can be left open for future ~~fine tuning~~fine-tuning, depending on the region.

For each day t, we consider the K best analogs, i.e. for which the distances are the smallest. We compute the spatial rank correlation between the Z500 best analogs and the Z500 at time t for ~~a posteriori~~ posterior verification purposes.

As a refinement over the study of Yiou and Déandréis (2019), a time embedding of τ days was used for the search of the analogs dates. This means that the field $X(t)$ for which we compute analogs is $X(t) = (Z500(t), Z500(t+1), \ldots, Z500(t+\tau))$. This ensures that temporal derivatives of the atmospheric field are preserved (Yiou et al., 2013). Hence the distance that is optimized to find analogs of the $Z500(x,t)$ field is:

$$D(t,t') = \left[\sum_x \left(\sum_{i=0}^{\tau} |Z500(x,t+i) - Z500(x,t'+i)|^2 \right) \right]^{\frac{1}{2}}, \quad (1)$$

where x is a spatial index, τ is the embedding time.

We consider different geographic domains as ~~showed~~ shown in Figure 1 for the computation of analogs and weather regimes. The computation of circulation analogs was performed with the "blackswan" Web Processing Service (WPS, Hempelmann et al. (2018)). The "blackswan" WPS is an online tool that helps ~~computing~~ compute circulation analogs on various datasets (reanalyses, climate model simulations) with a ~~user friendly~~ user-friendly interface.

3.2 Configuration of stochastic weather generator

We use a stochastic weather generator (SWG) based on a random sampling of the circulation analogs. The operation of the SWG and its design are detailed by Yiou and Déandréis (2019). The aim is to generate random trajectories from the previously computed analogs. Therefore, to generate a trajectory, we proceed as follows. For a given day t_0 in year y_0, we generate a set of $N = 100$ simulations until a time $t_0 + T$, with a lead time $T \in \{5, 10, 20\}$ days. We start at day t_0 and randomly select an analog (out of K analogs) of day $t_0 + 1$. The random selection of analogs of the day $t_0 + 1$ is performed with weights that are proportional to the calendar difference between t_0 and analog dates, to ensure that time goes forward. We also exclude analog dates with years that are equal to y_0. This rule is important for the next iterations. We then replace t_0 by the selected analog of

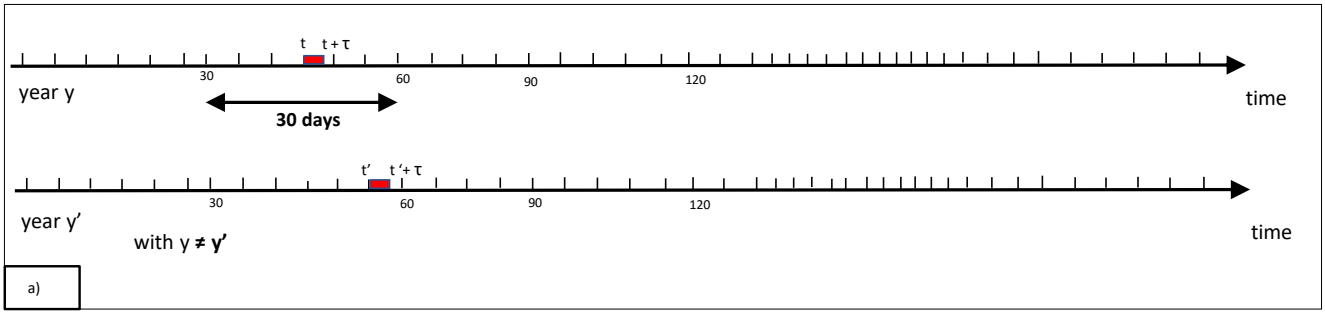

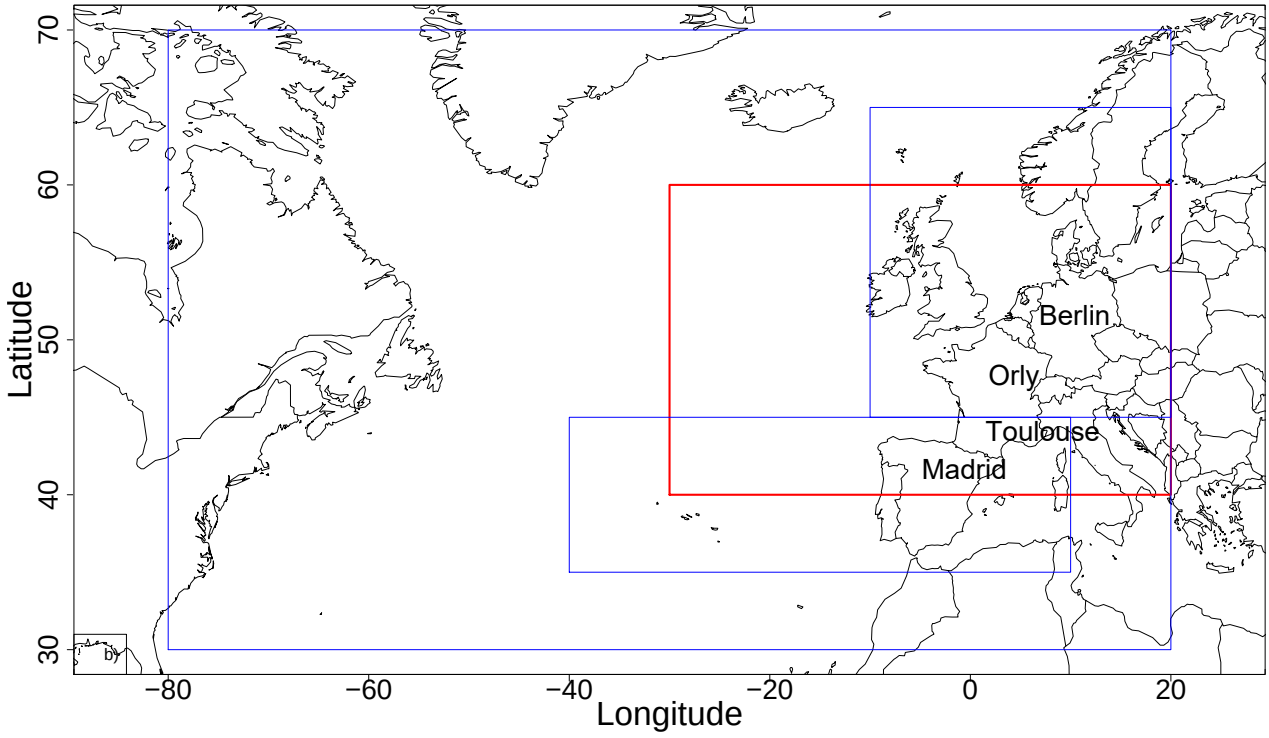

Figure 1. Parameters of the analog computation. (a) For each day t in year y, we chose an analog day t' with a similar sequence of τ consecutive day Z500 patterns. ~~t'~~ t_0 is selected within 30 calendar days of t ~~,~~and in a year ~~$y' \neq y$~~$y' \neq y$. (b) Domains of computation of analogs~~, we~~ . We computed analogs over different domains, each one ~~includes~~ including a part of the Atlantic and ~~focus in~~ focusing on a part of Western Europe, in order to test the sensitivity of our model to different geographic areas~~, the optimising~~ . The optimizing area was [30°W-20°E; 40°-60°N], indicated by the red rectangle.

$t_0 + 1$ and repeat the operation T times. Excluding ~~analog selection~~ analogs in year y_0 from the selection ensures that we do not use information from the T days that follow t_0. Hence, we obtain a hindcast trajectory between t_0 and $t_0 + T$.

~~This operation of trajectory simulation from~~ The procedure presented above is repeated $N = 100$ times to simulate $N = 100$ trajectories from t_0 to ~~$t_0 + T$ is repeated $N = 100$ times~~ $t_0 + T$. The daily precipitation of each trajectory is time-averaged between t_0 and $t0 + T$. Hence, we obtain an ensemble of $N = 100$ forecasts of the average precipitation for day t_0 and lead time T.

Then t_0 is shifted by $\Delta t \geq 1$ days, and the ensemble simulation procedure is repeated. This provides a set of ensemble forecasts with analogs.

We made a hindcast exercise, where the forecasts of precipitations based on analogs of atmospheric circulation (Z500), are started every $\Delta t \approx T/2$ day between January 1, 1948 and December 31, 2019. This yields a stochastic ensemble hindcast of precipitation and atmospheric circulation (Z500). In this paper, we~~therefore~~ , therefore, analyze the properties of an ensemble forecast of mean precipitation between t_0 and $t_0 + T$. To evaluate our forecasts, the predictions made with the SWG are compared to the persistence and climatological forecasts. The persistence forecast consists of using the average value between $t_0 - T$ and t_0 for a given year. The climatological forecast takes the climatological mean between t_0 and $t_0 + T$. The two "reference" forecasts are randomized by adding a small Gaussian noise, whose standard deviation is estimated by bootstrapping over T long intervals. We thus generate sets of persistence forecasts and climatological forecasts that are consistent with the observations (Yiou and Déandréis, 2019).

The simulations of this stochastic model will be called "SWG forecasts", as opposed to ECMWF forecasts.

3.3 Forecast Verification

Forecast verification is the process of determining the statistical quality of forecasts. A wide variety of ensemble forecast verification procedures exists (Jolliffe and Stephenson, 2011; **?**). They involve measures of the relationship between a set of forecasts and corresponding observations. To assess the quality of precipitation forecasts, we compute indicators such as the Correlation and Continuous Rank Probability Skill Score (CRPSS) for each lead time T, for different seasons and months.

The temporal rank correlation (referred as correlation skill) is calculated between the precipitation observations and the median of 100 simulations. This simple diagnostic is often used to assess forecast skills of indices (Scaife et al., 2014).

The continuous ranked probability score (CRPS) is widely used for ~~probability forecast verifications~~ probabilistic forecast verification (Ferro, 2007). It is sensitive to the distance between forecast and observation probability distributions.

If the ensemble forecast x yields a probability distribution $P(x)$ for a value x_a, the CRPS measures how the probability distribution of x compares with x_a (Hersbach, 2000).

The CRPS is computed as:

$$CRPS(P, x_a) = \int_{-\infty}^{+\infty} \left(P(x) - \mathcal{H}(x - x_a)\right)^2 dx, \tag{2}$$

where x_a is the observation and $\mathcal{H}$ is the Heaviside function of the occurrence of x_a ($\mathcal{H}(y) = 1$ if $y \geq 0$, and $\mathcal{H}(y) = 0$ otherwise). The decomposition and properties of the CRPS have been investigated by Ferro (2007), Hersbach (2000), and

Zamo and Naveau (2018). A perfect forecast would have a CRPS equal to 0, but the CRPS value obviously ~~depend~~ depends on the units of the variable to forecast, so ~~that~~ quantifying what is a "good" forecast requires a normalization. It is hence difficult to compare CRPS values for temperature and precipitation, within the same ensemble forecast. This issue is also acute for ~~non Gaussian~~ non-Gaussian variables with heavy tails (Zamo and Naveau, 2018) ~~,~~ so that the interpretation of a given CRPS value might not ~~always~~ be informative.

One way of circumventing this difficulty is to compare CRPS values to reference forecasts, such as persistence or climatology. The continuous rank probability skill score (CRPSS) is a normalization of Eq. (2) with respect to such a reference.

The CRPSS is hence computed by:

$$CRPSS = 1 - \frac{\overline{CRPS}}{\overline{CRPS_{ref}}} \tag{3}$$

where $\overline{CRPS}$ is the time average of the $CRPS$ of the SWG forecast and $\overline{CRPS_{ref}}$ is the time average of the $CRPS$ of the reference (either climatology or persistence). The CRPSS is interpreted as a fraction of improvement over a reference forecast.

The values of the CRPSS vary between $-\infty$ and 1. The forecast is considered to be an improvement over the reference when the CRPSS value is ~~close to 1 (i. e. when the CRPS is 0).~~ positive. Values of CRPSS equal to 0 indicate no improvement over the reference. Values inferior to 0 mean that the forecast is worse than the reference.

We use the CRPSS values to determine the maximum lead time T for which the SWG forecast is better than references. Then the SWG assessments will use the CRPS and directly compare the probability distributions of precipitation ensemble forecasts.

3.4 Dependence of forecast on weather regimes

We investigate the role of North Atlantic weather patterns on the forecast quality by attributing CRPS values of the SWG precipitation simulations to weather regimes. Weather regimes are defined as large-scale ~~quasi stationary~~ quasi-stationary atmospheric states. They are characterised by their recurrence, persistence and stationarity (Michelangeli et al., 1995). They help describing the features of the atmospheric circulation. Surface variables like temperature and precipitation are largely correlated with weather regimes (van der Wiel et al., 2019).

The North Atlantic weather regimes were computed with the procedure of Yiou et al. (2008), with the NCEP reanalysis. The first 10 principal components of SLP (large region in Figure 1b) are classified with a k-means algorithm onto four classes, over a reference period between 1970 and 2010. The procedure is repeated 100 times with random k-means initialization. Then we classify the resulting 100×4 k-means weather regimes, in order to determine the most probable classification. This heuristic procedure increases the robustness of the obtained weather regimes. Figure 2 shows four weather regimes for each season (winter and summer) that are coherent with the literature (Cassou et al., 2011; Ghil et al., 2008; Kimoto, 2001; Michelangeli et al., 1995)

The winter weather regimes are the ~~Scandinavian blocking (BLO~~negative phase of the North Atlantic oscillation (NAO-), Atlantic ridge (AR), ~~negative phase of the North Atlantic oscillation (NAO-)and Zonal flow~~ Scandinavian blocking (BLO), and Zonal (ZO). The summer weather regimes are the negative phase of the NAO (NAO-), ~~Atlantic ridge (AR~~Zonal (ZO),

Scandinavian blocking (BLO) and Atlantic low (AL). The regimes are not the same in both seasons, due to the seasonality of the ~~large scale~~ large-scale atmospheric circulation.

For each day (in winter and summer) between 1948 and 2019, we classify the SLP by minimizing the root mean square to four ~~reference~~ references (1970–2010) weather regimes.

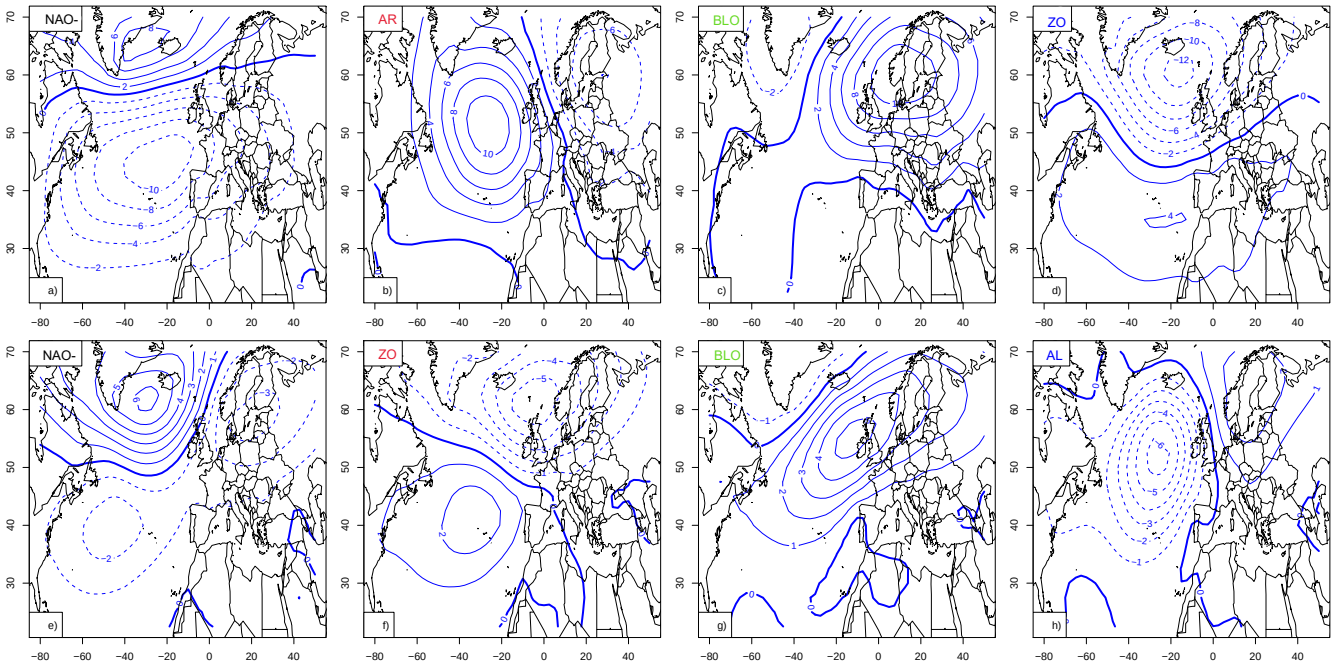

Figure 2. Weather regimes over Europe from SLP fields. Upper panels (a–d) contain winter (December-January-February: DJF) regimes: negative phase of the North Atlantic oscillation (NAO-), ~~the~~ Atlantic ~~ridge~~ Ridge (AR), ~~the~~ Scandinavian blocking (BLO), and ~~Atlantic zonal~~ Zonal regime (~~NAO+~~ZO). ~~The figure summarises the different states of the atmosphere during summer~~ Lower panels (~~a to d~~e–h) ~~and winter~~ contain summer (~~e to h~~June-July-August: JJA) ~~. It indicates the low and the high pressure over Europe and the direction~~ weather regimes: negative phase of ~~flow from~~ the ~~west~~ North Atlantic oscillation (NAO-), Zonal (ZO), Scandinavian blocking (BLO) and Atlantic Low (AL)~~to the east~~. The isolines show seasonal anomalies with respect to a ~~June-July-August~~ DJF and ~~December-January-February means~~JJA, in hPa with 2 hPa increments.

For each day t (within a given season), we consider the ~~analogs~~ analog dates of all $N = 100$ simulations between t and $t + T$ and the corresponding classification into weather regimes. Then we determine the most frequent weather regime of the N member ensemble forecast between t and $t + T$. We hence obtain ~~times~~ time series on the most likely weather pattern that dominates in the ensemble forecast between t and $t + T$.

We evaluate the influence of the dominating weather regimes on the SWG forecast quality by plotting the probability distribution of CRPS values ~~*conditional*~~*conditioned* ~~to each weather regime~~on the weather regimes. This is done separately for "good" forecasts (low CRPS values) and "poor" forecasts (high CRPS values).

We identify two classes of predictability from CRPS values:

- Low predictability is related to high values of CRPS that exceed the 75th quantile,
- High predictability is linked to low values of CRPS, below the 25th quantile.

Then we associate the dominating weather regimes computed above with classes of high or low predictability. This procedure helps identifying atmospheric patterns that could lead to low or high predictability with the SWG model.

4 ~~SWG~~ Stochastic Weather Generator parameter optimization

~~In order to obtain good forecast skill, we~~ We start by verifying the relationship between Z500 over the Euro-Atlantic region and the precipitation in the four studied areas, to ensure that Z500 analogs would be reasonable predictors of precipitation. We show the maps of the temporal rank correlation between the daily average of Z500 and the precipitation in Appendix B1. We ~~found~~ find a significant negative correlation between Z500 and the precipitation with p-values ≤ 0.05.

Then, we empirically adjust the parameters of the SWG simulations to ~~obtain better forecasts~~optimize the forecast scores. The first parameter is the geographical area. We computed sample trajectories of the SWG for the four domains outlined in Figure 1b. We used different domains in order to find an optimal region ~~which~~ that allows verifying the relationship between precipitation and Z500 for the four studied areas. Each domain includes a part of the Atlantic and a part of western Europe. We choose ~~a~~ the widest domain with the coordinates 80°W – 20°E and 30°– 70°N in order to catch the variability in the whole Euro-Atlantic region. However, ~~it gave poor~~ this large domain gave the poorest skill scores for precipitation forecasting for the studied areas as shown in Table 1. Then we focused on two smaller domains (outlined in blue in Figure 1b): one ~~centred~~ centered over northern Europe and the other ~~centred~~ centered over southern Europe. We found ~~good~~ better forecast skills for specific locations. ~~Same~~ The same level of performance was found for the domain (outlined in red in Figure 1b) with coordinates 30°W – 20°E and 40° – 60°N. Therefore, we kept this domain for the subsequent analyses, because it allows ~~to optimise~~ optimizing the correlations between Z500 and precipitation for the four studied areas and the time of computation of analogs at the same time. We compared the skill scores over the geographic domain with the coordinates 80°W – 20°E ; 30° – 70°N and 30°W – 20°E ; 40° – 60°N. We determined that the SWG simulations showed a better skill for the geographic domain (outlined in red in Figure 1b) and the skill scores remained the highest ones as represented in the following Table 1.

The second parameter is the number K of the best analogs that we use to simulate the precipitation. Our choice was based on numerical experiments. We performed different SWG simulations where we varied the number of analogs $K = 5, 10, 20$. We notice an improvement ~~on~~ in the skill scores by increasing the number of analogs as shown in table 2. Therefore, we considered $K = 20$ analogs to ensure that we have enough analog dates for the simulations. It appears that the Euclidean distance of analogs grows rather slowly after $K = 20$. Our choice was also comforted by a theoretical study by (Platzer et al., 2021) who showed that, for complex systems, the use of a large number of analogs ($K > 30$ analogs) does not change ~~much~~ the prediction properties with analogs. ~~Indeed,~~ Thus we kept $K = 20$ best analogs for the rest of the analyses.

Table 1. Correlation between observations and the median of 100 simulations for the winter (DJF) for the different studied domains represented in Figure 1b, with the coordinates 80°W – 20°E ; 30° – 70°N for the largest one (blue) and 30°W – 20°E ; 40° – 60°N for the red rectangle for a lead time of 5 days.

Location	**[80°W – 20°E ; 30° – 70°N] domain**		**[30°W – 20°E ; 40° – 60°N] domain**	
	Correlation	95% confidence interval	Correlation	95% confidence interval
Berlin	0.32	0.30 – 0. 35	0.50	0.48 – 0.56
Madrid	0.35	0.33 – 0. 39	0.53	0.51 – 0.55
Orly	0.39	0.37 – 0. 41	0.58	0.56 – 0.59
Toulouse	0.34	0.31 – 0.36	0.40	0.39 – 0.44

Table 2. CRPSS versus persistence and climatology for SWG simulations with 5, 10 and 20 analogs for the [30°W – 20°E ; 40° – 60°N] domain and for a lead time of 5 days.

Location	$K = 5$ **analogs**		$K = 10$ **analogs**		$K = 20$ **analogs**	
	Persistence	climatology	Persistence	climatology	Persistence	climatology
Berlin	0.29	0.20	0.39	0.31	0.56	0.50
Madrid	0.32	0.31	0. 40	0.39	0.57	0.57
Orly	0.34	0.12	0. 40	0.23	0.60	0.53
Toulouse	0.34	0.24	0.38	0.45	0.41	0.48

We quantify the dependence of the forecast on the time embedding for the analogs τ by calculating the analogs based on different embedding ~~going~~ values from $\tau = 1$ to 4 days. We find that an embedding of 4 days helped to better catch the persistence and improve the skill scores for the forecast compared to 1 day, as shown in Table 3. Therefore we kept the forecast based on a 4-day embedding. This choice was based on the numerical experiments performed for the studied locations. This is also supported by the study of Yiou et al. (2013), where the analog computation with ~~delays~~ time embedding was argued to improve the temporal smoothness of simulations. With such an embedding, forecasts for lead times of $T = 5$ days yield at least ~~two time~~ two-time increments.

For comparison purposes, SWG simulations are obtained using analogs computed from reanalyses on the NCEP and ERA5 reanalyses. By comparing their skill scores, we found that CRPSS and correlations between observations and simulations are positive in both cases, and ~~showing positive improvement comparing~~ show positive improvement compared to persistence and climatology forecasts. The CRPSS and correlation for simulations with analogs of NCEP are almost identical to those with ERA5, as shown in Table 4. Therefore, we focus on SWG simulations with analogs from the NCEP reanalysis in the sequel as both NCEP and ERA5 (1950 to 2019) have the same skill, as shown in Table 4, and because NCEP is easier to handle, ~~as its horizontal resolution is much lower~~due to its lower horizontal resolution. The computations were made using observations of

Table 3. Correlation between observations and the median of 100 simulations for the winter (DJF) based on analogs computed with an embedding of 1 and 4 days for the geographic domain with the coordinates 30°W – 20°E ; 40° – 60°N for a lead time of 5 days.

Location	$\tau = 1$ **day time embedding**		$\tau = 4$ **day time embedding**	
	Correlation	95% confidence interval	Correlation	95% confidence interval
Berlin	0.39	0.37 – 0. 43	0.50	0.48 – 0.56
Madrid	0.40	0.38 – 0. 42	0.53	0.51 – 0.55
Orly	0.42	0.39 – 0. 45	0.58	0.56 – 0.59
Toulouse	0.35	0.34 – 0.37	0.40	0.39 – 0.44

precipitation from the ECAD (Klein Tank et al., 2002) and E-Obs (Haylock et al., 2008) databases. We found the same results because the ECAD and E-Obs are highly correlated (by the construction of E-Obs).

Table 4. Comparison between the values of the CRPSS of SWG computed using different reanalysis dataset NCEP and ERA5 from 1979 to 2019 for a lead time of $T = 5$ days for winter (DJF)

Location	**CRPSS DJF (ERA5)**	**CRPSS DJF (NCEP)**
Berlin	0.50	0.50
Madrid	0.55	0.57
Orly	0.53	0.53
Toulouse	0.41	0.41

In summary, we made the forecast of the precipitation using $K = 20$ analogs computed from Z500 over the [30°W – 20°E; 40° – 60°N] domain (red rectangle in Figure 1 b). To compute analogs, we used NCEP reanalyses and an embedding of $\tau = 4$ days. The computations were based on ECAD observations (Klein Tank et al., 2002).

5 Results

5.1 Sample forecast

As an example, we illustrate the behavior of the trajectories in Orly for the summer and winter of 2002. Figure 3 shows the observed and simulated values of precipitation for lead times of 5 and 10 days for summer (June–July–August: JJA) and winter (December–January–February: DJF), for Orly precipitation data. We observe significantly positive correlations between observed values and the median of the forecasts, for the four data sets as represented in Table 5. The correlation is generally smaller in the summer than in the winter. The correlation skill is low for some ~~extremes~~ extreme values of precipitation. For a lead time of 10 days, SWG simulation still ~~show~~ shows a capacity to predict precipitation~~especially~~ , in particular for winter with a correlation equal to 0.23 (Orly), 0.30 (Berlin), 0.43 (Madrid), 0.31 (Toulouse).

Table 5. Correlation between observations and the median of 100 simulations for both seasons winter (DJF) and summer (JJA) for a lead time of 5 days

Location	Correlation DJF	95% confidence interval	Correlation JJA	95% confidence interval
Berlin	0.50	0.48 – 0.56	0.22	0.21 - 0.23
Madrid	0.53	0.51 – 0.55 - 0.59	0.29	0.27 - 0.30
Orly	0.58	0.56 – 0.59	0.23	0.20 - 0.24
Toulouse	0.40	0.39 – 0.44	0.18	0.15 - 0.19

We observe that the 5th and 95th quantiles of the simulations include the different values of observations. This heuristically confirms the good skill of SWG to forecast precipitation from Z500 for several seasons (winter and summer) in several locations for $T = 5$ and $T = 10$ day lead times.

The difference ~~of~~ in the forecast correlation skills between the four studied locations may be related to the variation of the local climate from one region to ~~an other~~another. The studied areas are in different climate types according to the Köppen-Geiger ~~'s climate classification map~~ climate classification (Peel et al., 2007). From the ~~south western~~ southwestern side of Europe, Madrid is in the arid zone of the classification (Peel et al., 2007), which indicates that convective rains are less ~~significant, so that~~ frequent, and the origin of precipitation might be the result of humidity coming from the Atlantic. Conversely, Berlin is located in a cold zone ~~characterised~~ characterized by warm summer and the absence of a dry season (Peel et al., 2007)~~, so that~~ ; the precipitation could be the result of both convective rains and Atlantic humidity.

In this paper, we decided (for simplicity) to use the same analogs to forecast precipitation for those four stations as discussed in section 4. A refinement of the analog regions would be necessary when focusing on Madrid vs. Berlin.

5.2 Forecast probability skill

The CRPSS and correlation skill scores are computed for the four studied stations (Orly Berlin, Madrid and Toulouse), as shown in ~~illustrations represented in (Figure 4)~~ Figure 4 and for lead times from 5 to 20 days. ~~We represent skill scores for January and July in order to show the skill of the SWG to predict precipitation in different conditions.~~

In this paper, we choose to present the results for summer and winter, to highlight the capacity of the SWG to forecast the precipitation in extreme seasons. We focus on January and July in order to show the skill of the SWG to predict precipitation in different conditions.

The CRPSS against the persistence and climatology references show positive values for lead times of up to 20 days (Figure 4). The values of CRPSS against the persistence reference (represented by squares) decrease with lead times in winter for the different studied areas, showing high values over 5 days. However, for summer, we notice that the values of CRPSS against persistence increase with lead time, with high values over 20 days expect for Berlin. ~~That indicates that for the summer until 20 days the~~ This indicates that the SWG forecast is still better than the persistence forecast (the average of the CRPS of SWG is smaller than the average of the CRPS of the persistence) for lead times of 20 days in the summer. ~~That could be explain~~

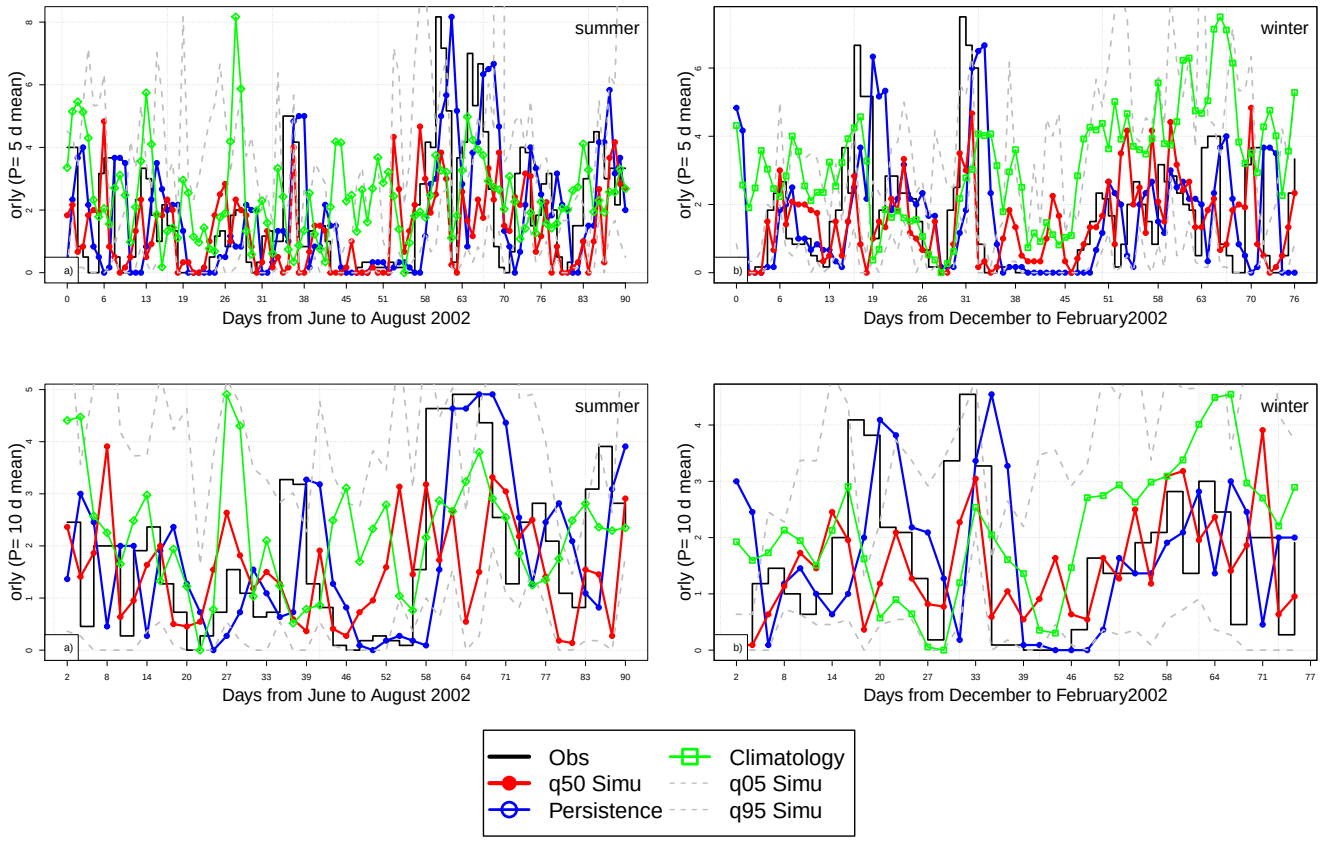

Figure 3. Time series of analog ensemble forecasts for 2002, for lead times of 5 days (top) and 10 days (bottom) for summer (June to August) a) and c) and winter (December to February) b) and d) for Orly. The median of 100 simulations is represented by the red line. ~~Black~~ The black line ~~represent observations~~ represents observation values. Gray lines represent the 5th and 95th quantiles. ~~Blue lines represent~~ The blue line represents the persistence forecasts and the green ~~lines represent~~ line represents the climatology forecasts. The y-axis ~~represent~~ represents the average ~~of~~ precipitation over ~~$T = 5, 10$~~ $T = 5, 10$ days.

This could be explained by the fact that summer precipitation in Orly (51% of the time, on average) comes in clusters contrary to precipitation in Berlin. Indeed, we computed the seasonal frequency of precipitation (defined as the number of days when precipitation exceeds 0.5 mm/day). We found that for Berlin, precipitation exceeding 0.5 mm/day is more frequent than in the other stations (close to 50% of the time for both seasons).

This means that a persistence forecast for Orly is likely to be skillful, even for longer lead times, especially in the summer. Therefore, the trends in CRPSS values for different lead times are probably due to the intrinsic time persistence of local precipitation.

The CRPSS against the climatology reference (triangles) ~~show~~ shows lower values compared to the CRPSS against persistence reference, although they are positive for all lead times and for both seasons. However, we notice that for a short lead time the SWG is better than the climatology.

The correlation skill is positive for both seasons but higher in winter (January) than in summer (July). For a lead time of 5 days, the correlation is equal to 0.59 for Madrid, 0.50 for Berlin and ~~to~~ 0.40 for Toulouse. For a lead time of 10 days, it is equal to 0.42 for Madrid, 0.30 for Berlin and ~~to~~ 0.41 for Toulouse.

The SWG was tested by Yiou and Déandréis (2019) to forecast temperature in western Europe. Comparing the performance of the SWG to forecast those different meteorologic variables, we notice that the model shows good performance to forecast the temperature in the winter, also the best performance of the model is at a lead time of 5 days. We find that the skill scores (CRPSS and correlation) decrease with lead times. The forecast skill of the SWG shows variability from one location to another. However, the model was able to forecast temperature until 40 days in Berlin, Orly and Toulouse with positive skill scores.

From a visual inspection of the CRPSS and correlations, we chose to focus on lead times of $T = 5$ days, for which the correlation exceeds 0.5 in the winter. It is rather low in the summer, due to convective events leading to a high precipitation variability (from no rain to very high values). Correlation scores become barely significant for lead times of 20 days, so that, like temperature, the SWG should not be used beyond that horizon.

5.3 Relation between weather regimes and CRPS

We investigate the role of North Atlantic weather patterns defined in Section 3.4 (Figure 2) on the forecast skill of the SWG precipitation simulations.

We start by comparing the frequencies of the weather regimes from the observations and the most frequent weather regime found in SWG simulations for a given lead time $T = 5$ days. We find that the percentages are very similar (Figure 5). This means that the weather regimes of the simulated trajectories do not yield major biases for the summer or winter seasons.

Then we look at the relation between weather ~~regime and the CRPS~~ regimes and CRPS values, by using the most frequent weather regime within T days and the two classes of quantiles of the CRPS that related to good quality of forecast (attributed to low values of CRPS $\leq q_{25}$) and poor quality of forecast (attributed to high values of CRPS $\geq q_{75}$). This relation is represented in Figure 6 for Orly and for the rest of the studied stations in Figure A1. We find a small influence of specific weather regimes on the CRPS distribution for summer.

The weather regime signal for "good" forecasts depends on the season and the considered station. When the forecast has a low CRPS value (for Orly), we find that the Scandinavian Blocking regime slightly dominates (green bar in Figure 6a, b). This is also the case for Berlin (in winter) and Toulouse Figure A1 (b, j). The low CRPS values in Madrid are obtained for the Atlantic Ridge regime Figure A1 f.

The weather regime signal for "poor" forecasts also yields a dependence on the season and station. Higher CRPS values are obtained with the ~~Atlantic Ridge~~ Zonal regime in the summer for Orly (red line in Figure 6 c) and ~~Berlin in winter and summer~~Toulouse. The Atlantic ridge regime favors high CRPS values (i.e. poor forecasts) for Madrid in winter Figure A1 h. The ~~Atlantic ridge regime~~ Scandinavian Blocking favors high CRPS values for ~~Toulouse in summer~~Berlin in in winter and

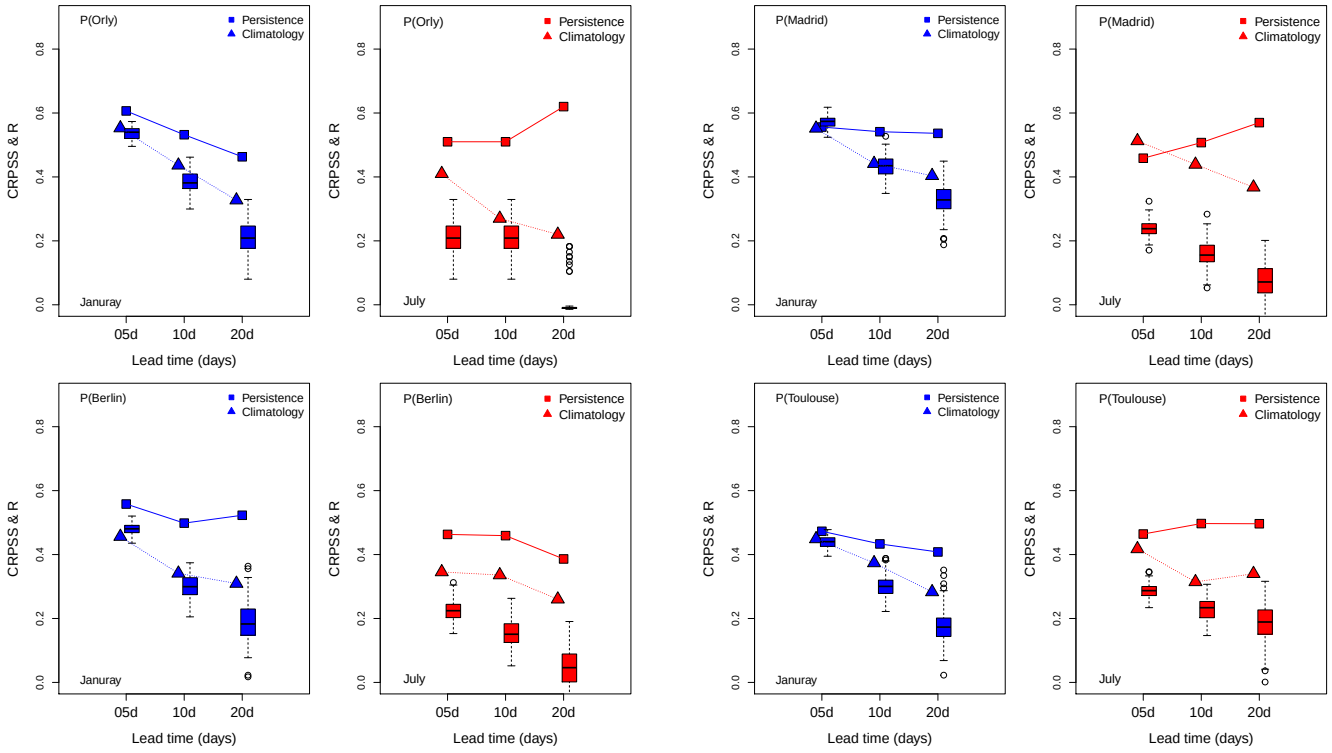

Figure 4. Skill scores for the precipitation of Orly, Madrid, Berlin and Toulouse for lead times of 5, 10, 20 days for January (blue) and July (red) for analogs computed from reanalyses of (a) NCEP and (b) ERA5. Squares indicate CRPSS where the Persistence is the baseline, triangles ~~indicates~~ indicate CRPSS where the climatology is the reference, and boxplots ~~indicates~~ indicate the probability distribution of correlation between observation and the median of 100 simulations for all days. The boxplot upper whisker is: ~~$\min\{1.5(q_{75}-q_{50})+q_{50}, \max(CRPS)\}$~~ $\min\{1.5(q_{75}-q_{50})+q_{50}, \max(CRPSS)\}$. The boxplot lower whisker is: ~~$\max\{q_{50}-1.5(q_{75}-q_{50}), \min(CRPS)\}$~~ $\max\{q_{50}-1.5(q_{75}-q_{50}), \min(CRPSS)\}$.

summer (green line in Figure A1 c and d). The different impacts of the weather regimes on the studied areas ~~is~~ are related to the position of the high and ~~low pressure~~ low-pressure regions of each weather regime ~~and their position regarding~~ in the studied areas.

This relation between predictability (or the CRPS distribution) and weather regimes, albeit weak, is consistent with previous work of Faranda et al. (2017). Similar ~~relation~~ relations were found between weather regimes over Europe and the Temperature in a recent study by Ardilouze et al. (2021). We find that the sensitivity of the forecast to weather regime is larger for low values of CRPS and in ~~the~~ winter. The sensitivity of forecast skill to weather regimes is rather small on average, even for ~~low lead times~~ small lead times ($T = 5$ days).

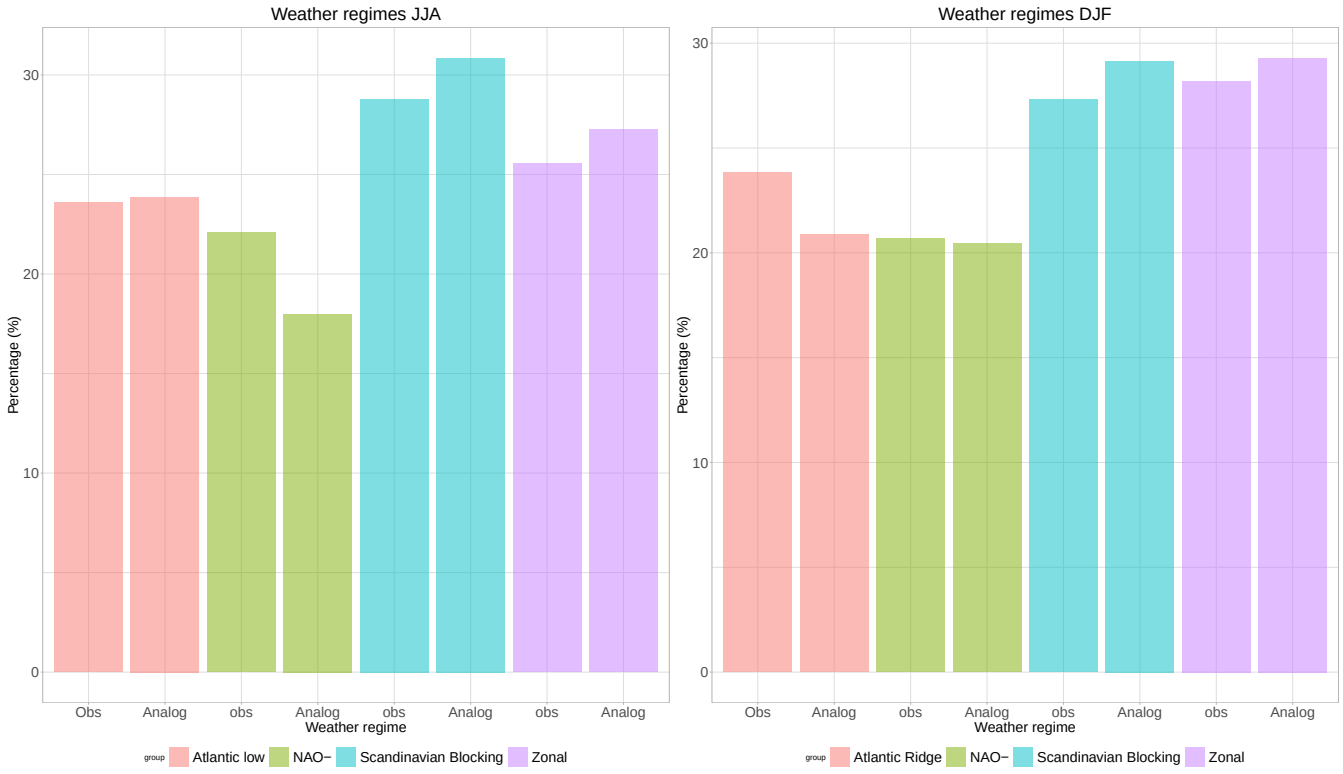

Figure 5. Percentage of each weather regime for observations dates (Obs) and the most frequent weather regime from SWG simulations between t_0 and $t_0 + T = 5$ days (Analog) over the period from 1948 to 2019 for summer (JJA: left panel) and winter (DJF: right panel). The percentage of weather regime ~~are~~ is the same in Obs and Analog.

5.4 Comparison with ECMWF forecast

We first compared the CRPSS of SWG forecasts for winter and summer with the CRPSS of ECMWF forecasts.

The CRPSS of the ECMWF forecast is computed for different lead times going from 1 day to 10 day for precipitation (Haiden et al., 2018) over the region 12.5°W – 42.5°E ; 35.0° – 75.0°N (ECMWF, 2020). It uses the climatology as a reference (Haiden et al., 2018). The values of CRPSS for Europe for 2020 decrease with lead times (Haiden et al., 2018). The CRPSS of ECMWF is about 0.16 in summer (JJA) and 0.25 in winter (DJF) for a lead time of $T = 5$ days (ECMWF, 2020). The CRPSS of SWG simulations for a lead time of $T = 5$ days is shown in Table 4. The values suggest that the predictive skill of SWG is qualitatively promising for short lead times, compared with ECMWF forecasts. However, we have to mention that the values of CRPSS for ECMWF are computed over all of Europe for both seasons (Haiden et al., 2018) while with the SWG we are doing a forecast for local stations.

We made a quantitative comparison between the two forecasts for the different lead times. We computed the CRPS for the ECMWF ~~forcast~~forecast. Then, we used the Kolmogorov-Smirnov (KS) test (von Storch and Zwiers, 2001, Chap.1) to

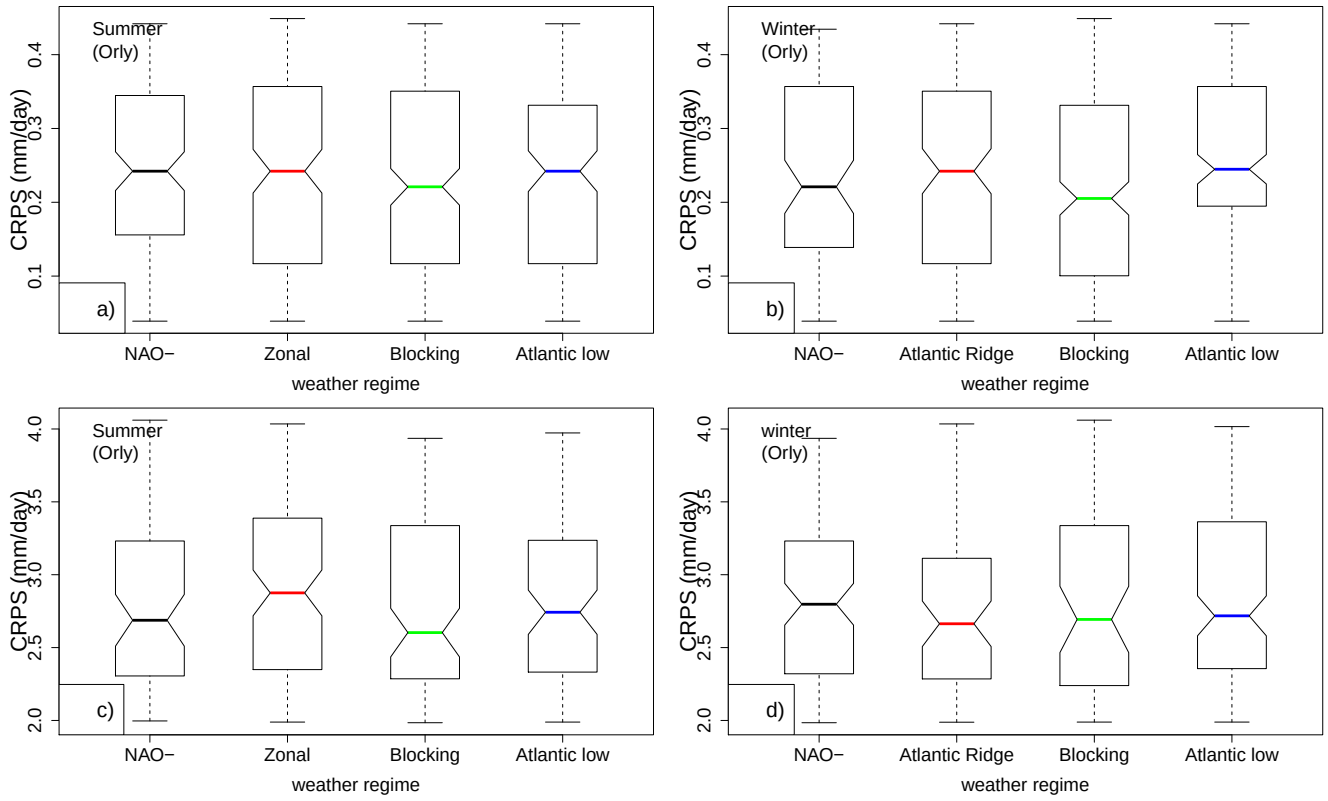

Figure 6. Relation between CRPS and weather regimes for Orly, for SWG forecasts with lead time $T = 5$ days. Upper panels (a and b): CRPS value distribution conditioned on four weather regimes, when CRPS is lower than q_{25}. lower panels (c and d): CRPS is higher than q_{75}. The boxplots indicate the median (q_{50}) of the distribution (thick bar). 25th (q_{25}) and 75th (q_{75}) quartiles (lower and upper segments). The boxplot upper whisker is: $\min\{1.5(q_{75} - q_{50}) + q_{50}, \max(CRPS)\}$. The boxplot lower whisker is: $\max\{q_{50} - 1.5(q_{75} - q_{50}), \min(CRPS)\}$.

compare the probability distributions of the CRPS of SWG and ECMWF forecasts. The null hypothesis supposes that the CRPS of ECMWF and SWG forecasts have the same distribution. The null hypothesis of the KS test was rejected~~, which~~ ; this means that the two ~~times~~ time series do not have the same distribution~~with a p.values~~ , with a p-value $= 0.11$. A similar result was found by Ardilouze et al. (2021), where they compared the efficiency between ECMWF and CNRM forecasts.

We found that 80%, 39% 50% and 40 % of the CRPS of SWG forecast are equal to zero for respectively Orly, Berlin, Madrid and Toulouse, for a lead time of $T = 5$ days ~~(Figure 7)~~Figure 7, which shows the capacity of the SWG to well simulate rain events. One notable difference between SWG and ECMWF forecasts is that although the proportion of CRPS values close to zero is higher ~~in~~ for ECMWF, the CRPS for the worst forecasts ~~are~~ is much higher than those of SWG. Indeed, we notice that the time average of CRPS of ECMWF (blue vertical lines) and SWG (red vertical lines) for $T = 5$ days are close, with higher values for ECMWF Figure 7. However, the median ~~of~~ CRPS of ECMWF ~~are~~ is smaller compared to the SWG (dashed vertical

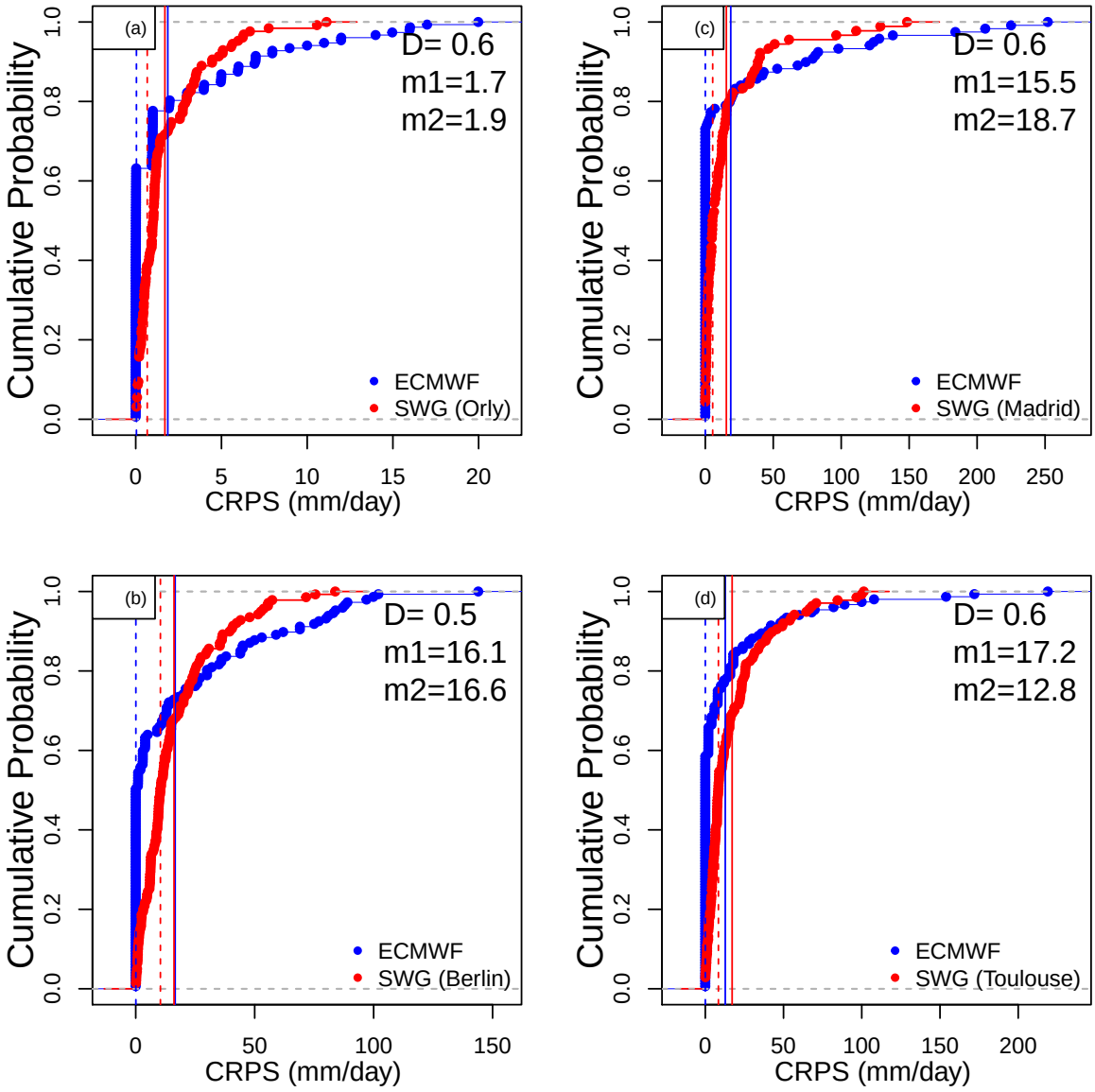

Figure 7. Empirical cumulative distribution function of the CRPS of ECMWF (blue) and SWG (red) forecasts for 5 days for Orly (a), Berlin (b), Madrid (c) and Toulouse (d). D is the maximum distance between both ECDFs (value of Kolmogorov-Smirnov test). $m1$ is the value of the time average of CRPS of SWG and $m2$ is the value of the time average of CRPS of ECMWF. The vertical dashed lines represent the median of CRPS of ECMWF (blue) and SWG (red).

lines) 7. Finally, we computed the CRPSS for ECMWF forecasts taking as a reference the CRPS of SWG (Table 6). We hence compute the CRPSS of ECMWF forecast by normalizing the CRPS by the CRPS of SWG forecast in Eq. (C1).

Table 6. CRPSS of ECMWF forecasts using as a reference the CRPS of SWG, for lead times of ~~$T = 5$~~T = 5, 10 and 20 days. It shows that the SWG has a positive improvement ~~comparing~~ compared to the ECMWF forecast as the CRPSS are above zero, ~~expect~~ except for Toulouse.

Location	**Orly**	**Berlin**	**Madrid**	**Toulouse**
CRPSS $T = 5$ **days**	-0.09	-0.02	-0.2	0.25
CRPSS $T = 10$ **days**	-0.17	-0.54	-0.33	0.23
CRPSS $T = 20$ **days**	-0.50	-0.36	-0.1	-0.08

This evaluates the added value of the ECMWF forecast over the SWG forecast. We find that the ECMWF forecast has no improvement over the SWG forecast for the different lead times because the CRPSS ~~value~~ values are negative. At $T = 5$ days, we notice that the improvement is negligible for Orly and Berlin, while it is much better for Madrid. However, for Toulouse, the ECMWF forecast still ~~have~~ has better skills for lead times of $T = 5, 10$ days. For a lead time of $T = 10$ days, the improvement of the SWG forecast over the ECMWF is important~~especially~~ , particularly for Berlin and Madrid. There is a major improvement for a lead time of $T = 20$ days for Orly and Berlin. ~~This confirm~~

This confirms the relatively good skill of the SWG to forecast precipitation, compared to ECMWF. ~~And that~~ This could be explained by the difference ~~on~~ in the average of the CRPS of the two forecasts. Indeed, as we mentioned before, the ECMWF forecast ~~has good skill~~ yields best skill scores for small values of precipitations ~~, we further explained that on~~ (< 2 mm/day). We further illustrate those comparisons in the Annexes (Figure C1 and Table C1).

6 Conclusions

In this work, we have shown the performance of a stochastic weather generator (SWG) to simulate precipitation over different locations in western Europe and for various ~~times~~ time scales from 5 to 20 days. The input of our model was analogs of geopotential heights at 500 hPa (Z500). The choice of such input was made in order to evaluate the impact of ~~large scale~~ large-scale circulation on local weather variables. SWG showed a good skill to predict precipitation for a lead time of 5 and 10 days from ~~analogues~~ analogs of Z500.

This study of precipitation forecast complements the work of Yiou and Déandréis (2019) ~~, for precipitation~~initially made to forecat temperature and NAO index. We explored the sensitivity of the SWG model on analogs computed from different geographical areas and from different reanalyses (ERA5 and NCEP). We found that ~~the~~ both NCEP and ERA5 reanalyses provide good performances for simulations~~, due to its longer length ($\approx$ 70 years in NCEP and ERA5). Therefore the length of the analog database does make a difference, as already suggested by Jézéquel et al. (2018a).~~ .

We evaluated the relation between the quality of the forecast and weather regimes over Europe~~, we~~ . We found that low and high predictability was related to specific weather regimes~~, this~~ . This dependence is more significant in winter than in summer~~, especially for the good predictability , it is found to be~~ . We found that good predictability is mainly related to Blocking.

A comparison with the ECMWF forecast system over Western Europe confirmed ~~the good performance~~ quantitatively and qualitatively the skill forecast of the SWG ~~quantitatively and qualitatively~~, for lead times $T \leq 10$ days. Of course, the SWG

model cannot replace a numerical weather prediction, as the SWG parameters (e.g. region of analogs) need to be tuned to local variables, and rely on the existence of a fairly large database to compute analogs. Here we used the same domain of circulation analogs for stations from Madrid to Berlin. Obviously, this region should be optimized for each individual station. Therefore, the main utility of the SWG forecast system is to make local ensemble simulations, where its performances can challenge a numerical weather prediction ~~,~~if the parameters are ~~well tuned~~well-tuned.

This paper hence confirms the proof of concept to generate ensembles of (local) precipitation forecasts from analogs of circulation. Its performance relies on the relation between precipitation and the synoptic atmospheric circulation, which is verified for western Europe. Transposing this SWG to other regions of the globe requires observations covering several decades. Numerical weather models obviously do not yield this constraint.

Code availability. The code and data files are available at http://doi.org/10.5281/zenodo.4524562

Author contributions. MK performed the analyses. PY co-designed the analyses. CD and ST participated to the manuscript preparation.

Competing interests. The authors declare no competing interest.

Acknowledgements. This work is part of the EU International Training Network (ITN) Climate Advanced Forecasting of subseasonal Extremes (CAFE). The project receives funding from the European Union's Horizon 2020 research and innovation programme under the Marie Skłodowska-Curie Grant Agreement No 813844. We thank L. Magnusson and F. Pappenberger for helpful discussions on the ECMWF data.

Appendix A: CRPS and weather regimes

To avoid a tedious redundancy we deferred the figures of evaluation of the forecast quality by weather regimes to this appendix section.

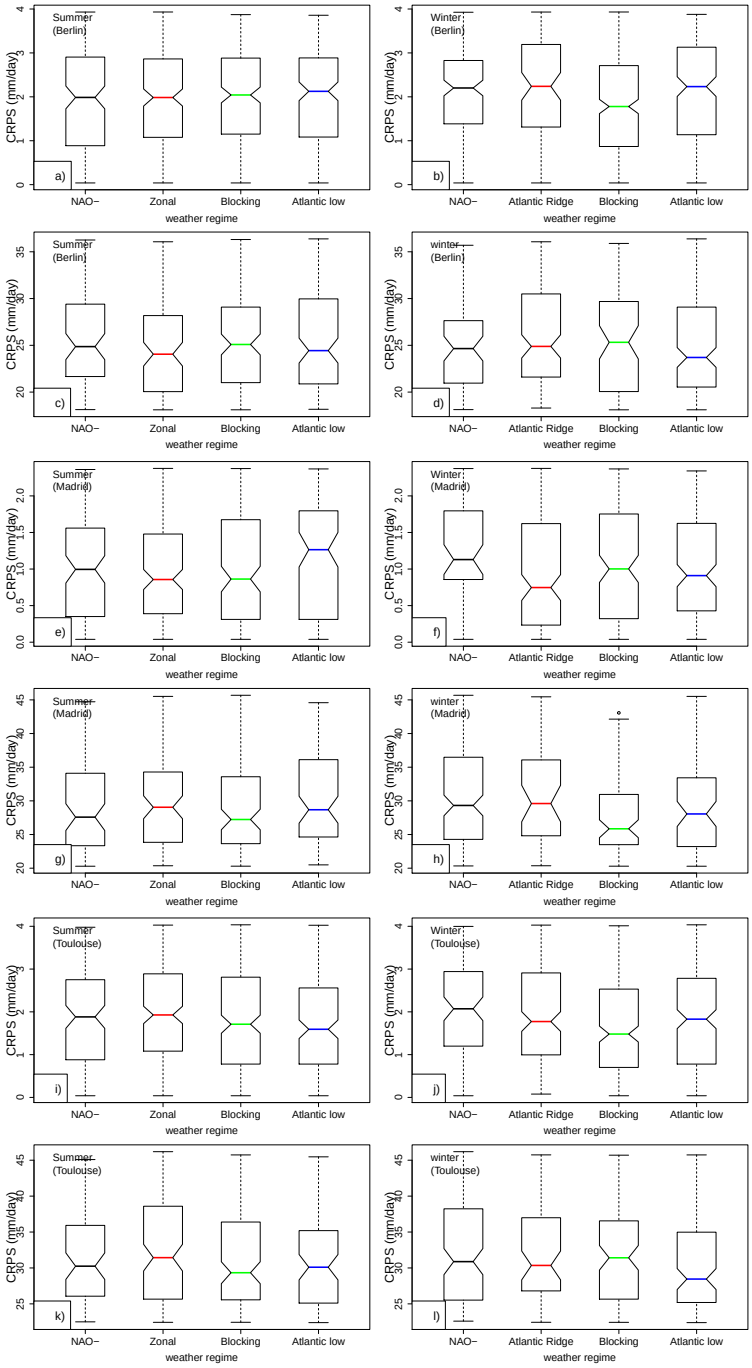

Figure A1. Relation between CRPS and weather regimes for Berlin (a–d)), Madrid (e–h) and Toulouse (i–l), for SWG forecasts with lead time $T = 5$ days. The panels (a, b, e, f, i and j) correspond to CRPS value distribution conditioned on four weather regimes, when CRPS is lower than q_{25}. The panels (c, d , g, h, k and l) correspond to a higher CRPS value $CRPS \geq q_{75}$. The boxplots indicate the median (q_{50}) of the distribution (thick bar).

Appendix B: Relation between Z500 and precipitation

In order to justify, the use of the Z500 as a driver of precipitation. We computed the rank spatial correlation between the daily average of Z500 over the Euro Atlantic region and the precipitation in each studied station (Madrid, Berlin,Toulouse and Orly). We did the analysis for different seasons (DJF ~~-~~and JJA). We find a maximum correlation amplitude of ~~-0.5~~ -0.5 for Madrid and Orly, and a correlation of ~~-0.4 and -0.3~~ -0.4 and -0.3 respectively for Toulouse and Berlin. The correlation is significant as we have a p.value < 0.05 for the different grid points. This indicates the relation between Z500 patterns and precipitation~~especially in western Europe~~ , in particular in western Europe, and that a decrease in Z500 is linked with precipitation.

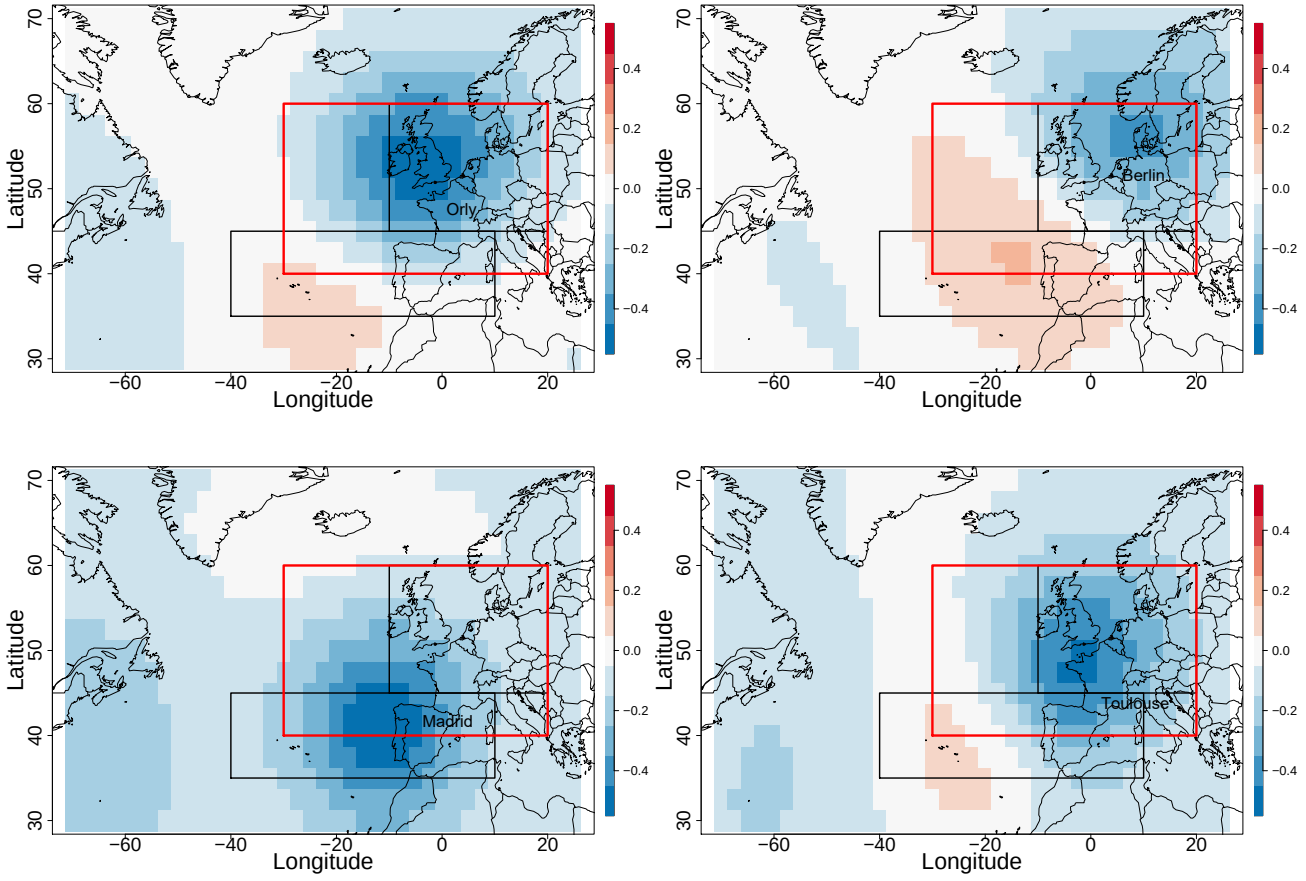

Figure B1. Maps of correlation between Z500 and precipitation in Berlin, Madrid, Orly and Toulouse for the period from 1948 to 2019 over the Euro-Atlantic region. The rectangles represent the domains of computation of analogs. We highlight the optimized area [30°W-20°E; 40°-60°N] by the red rectangle.

Appendix C: CRPSS of ECMWF versus SWG

We explain further the comparison that we made between the ECMWF forecast and the SWG forecast. As mentioned we found that the SWG has ~~improvement comparing to~~ improved compared to the ECMWF forecast. This is related to the difference ~~on~~ in the time average of the CRPS of the two forecasts. We computed the CRPSS as ~~follow~~follows:

$$CRPSS = 1 - \frac{\overline{CRPS_{ECMWF}}}{\overline{CRPS_{SWG}}} \tag{C1}$$

with $\overline{CRPS_{ECMWF}}$ is the time average of the $CRPS$ of the ECMWF forecast and $\overline{CRPS_{SWG}}$ is the time average of the $CRPS$ of the SWG.

Table C1. CRPSS, average and median of CRPS of ECMWF and SWG forecasts for lead times of $T = 5$, 10 and 20 days. It shows that the CRPS of SWG forecast has a smaller average than the CRPS of ECMWF ~~forcast~~forecast, which explains the values of CRPSS for the different studied areas and the positive improvement of the SWG compared to ECMWF.

Location	**Orly**	**Berlin**	**Madrid**	**Toulouse**
$\overline{CRPS_{ECMWF}}$ / Median	1.87 / 0.04	16.56 / 0.05	18.73 / 0.003	12.76 / 0.01
$\overline{CRPS_{SWG}}$ / Median	1.70 / 0.67	16.10 / 10.37	15.49 / 5.45	17.16 / 8.39
CRPSS $T = 5$ days	**-0.09**	**-0.02**	**-0.2**	**0.25**
$\overline{CRPS_{ECMWF}}$	1.70 / 0.05	18.1 / 0.06	20.03 / 0.1	14.87 / 0.09
$\overline{CRPS_{SWG}}$	1.44 / 0.78	11.67 / 5.45	15.04 / 6.13	19.45 / 7.89
CRPSS $T = 10$ days	**-0.17**	**-0.54**	**-0.33**	**0.23**
$\overline{CRPS_{ECMWF}}$	1.67 / 0.1	13.54 / 0.09	17.89 / 0.1	17.8 / 0.08
$\overline{CRPS_{SWG}}$	1.11 / 0.9	9.91 / 6.3	16.23 / 5.89	16.41 / 8.34
CRPSS $T = 20$ days	**-0.50**	**-0.36**	**-0.1**	**-0.08**

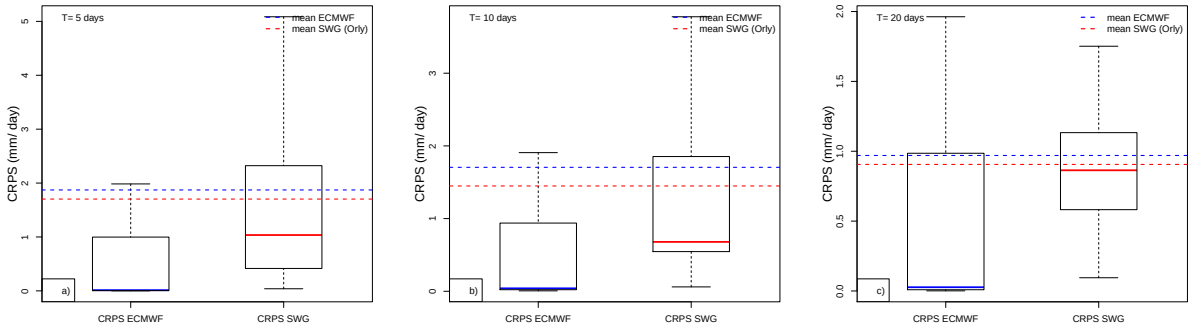

Figure C1. Boxplots of CRPS of ECMWF and CRPS of SWG for Orly, with lead time ~~$T = 5, 10, 20$~~ $T = 5$, 10 and 20 days. The boxplots indicate the median (~~q_{50}~~q50) of the distribution (thick bar blue for ECMWF and red for SWG). 25th (~~q_{25}~~q25) and 75th (~~q_{75}~~q75) quartiles (lower and upper segments). The upper whisker is ~~$\min\{\max(X), q_{50} + 1.5(q_{75} - q_{25})\}$~~$\min\{\max(X), q50 + 1.5(q75 - q25)\}$. We ~~indicates also~~ indicate the average ~~of~~ CRPS of ECMWF and SWG forecasts with horizontal ~~dash~~ dashed lines. We notice ~~clearly~~ that the distribution is asymmetric as the median and the average are unequal. ~~And that the~~ The average ~~of~~ CRPS for SWG forecast is lower than the average ~~of~~ CRPS for ECMWF forecast. We do not show the outliers that are above the upper whiskers.

References

Ailliot, P., Allard, D., Monbet, V., and Naveau, P.: Stochastic weather generators: an overview of weather type models, Journal de la Société Française de Statistique, 156, 101–113, 2015.

Ardilouze, C., Specq, D., Batté, L., and Cassou, C.: Flow dependence of wintertime subseasonal prediction skill over Europe, preprint, Atmospheric predictability, https://doi.org/10.5194/wcd-2021-32, https://wcd.copernicus.org/preprints/wcd-2021-32/, 2021.

Atencia, A. and Zawadzki, I.: A comparison of two techniques for generating nowcasting ensembles. Part I: Lagrangian ensemble technique, Monthly Weather Review, 142, 4036–4052, 2014.

Blanchet, J., Stalla, S., and Creutin, J.-D.: Analogy of multiday sequences of atmospheric circulation favoring large rainfall accumulation over the French Alps, Atmospheric Science Letters, 19, e809, https://doi.org/10.1002/asl.809, http://doi.wiley.com/10.1002/asl.809, 2018.

Cassou, C., Minvielle, M., Terray, L., and Périgaud, C.: A statistical–dynamical scheme for reconstructing ocean forcing in the Atlantic. Part I: weather regimes as predictors for ocean surface variables, Climate Dynamics, 36, 19–39, https://doi.org/10.1007/s00382-010-0781-7, http://link.springer.com/10.1007/s00382-010-0781-7, 2011.

Eckmann, J.-P. and Ruelle, D.: Ergodic theory of chaos and strange attractors, in: The Theory of Chaotic Attractors, pp. 273–312, Springer, 1985.

ECMWF: European Centre for Medium-Range Weather Forecasts, https://apps.ecmwf.int/webapps/opencharts/products/plwww_3m_ens_tigge_wp_mean?area=Europe&parameter=24h:20precipitation&score=CRPSS, accessed:2021-02-03, 2020.

Faranda, D., Messori, G., and Yiou, P.: Dynamical proxies of North Atlantic predictability and extremes, Scientific reports, 7, 41 278, https://www.nature.com/articles/srep41278.pdf, 2017.

Ferro, C. A. T.: A probability model for verifying deterministic forecasts of extreme events, Weather and Forecasting, 22, 1089–1100, <GotoISI>://000250413300011, 2007.

Gabriel, K. R. and Neumann, J.: A Markov chain model for daily rainfall occurrence at Tel Aviv, Quarterly Journal of the Royal Meteorological Society, 88, 90–95, 1962.

Ghil, M., Chekroun, M., and Simonnet, E.: Climate dynamics and fluid mechanics: Natural variability and related uncertainties, Physica D, 237, 2111–2126, https://doi.org/10.1016/j.physd.2008.03.036, 2008.

Haiden, T., Janousek, M., Bidlot, J., Buizza, R., Ferranti, L., Prates, F., and Vitart, F.: Evaluation of ECMWF forecasts, including the 2018 upgrade, European Centre for Medium Range Weather Forecasts, 2018.

Haylock, M. R., Hofstra, N., Tank, A. M. G. K., Klok, E. J., Jones, P. D., and New, M.: A European daily high-resolution gridded data set of surface temperature and precipitation for 1950-2006, J. Geophys. Res. - Atmospheres, 113, doi:10.1029/2008JD010 201, <GotoISI>://000260598000009, 2008.

Hempelmann, N., Ehbrecht, C., Alvarez-Castro, C., Brockmann, P., Falk, W., Hoffmann, J., Kindermann, S., Koziol, B., Nangini, C., Radanovics, S., Vautard, R., and Yiou, P.: Web processing service for climate impact and extreme weather event analyses. Flyingpigeon (Version 1.0), Computers & Geosciences, 110, 65–72, https://doi.org/10.1016/j.cageo.2017.10.004, https://github.com/bird-house/blackswan, 2018.

Hersbach, H.: Decomposition of the Continuous Ranked Probability Score for Ensemble Prediction Systems, WEATHER AND FORECASTING, 15, 12, 2000.

Hersbach, H., Bell, B., Berrisford, P., Hirahara, S., Horányi, A., Muñoz-Sabater, J., Nicolas, J., Peubey, C., Radu, R., and Schepers, D.: The ERA5 global reanalysis, Quat. J. Roy. Met. Soc., 146, 1999–2049, 2020.

Jolliffe, I. T. and Stephenson, D. B.: Forecast verification: a practitioner's guide in atmospheric science, John Wiley & Sons, 2011.

Jézéquel, A., Yiou, P., and Radanovics, S.: Role of circulation in European heatwaves using flow analogues, Climate Dynamics, 50, 1145–1159, 2018a.

Jézéquel, A., Yiou, P., Radanovics, S., and Vautard, R.: Analysis of the exceptionally warm December 2015 in France using flow analogues, Bulletin of the American Meteorological Society, 99, S76–S79, 2018b.

Kimoto, M.: Studies of Climate Variability Using General Circulation Models, in: Earth Planets and Space, 2001.

Kistler, R., Kalnay, E., Collins, W., Saha, S., White, G., Woollen, J., Chelliah, M., Ebisuzaki, W., Kanamitsu, M., Kousky, V., van den Dool, H., Jenne, R., and Fiorino, M.: The NCEP-NCAR 50-year reanalysis: Monthly means CD-ROM and documentation, Bulletin of the American Meteorological Society, 82, 247–267, <GotoISI>://000166742900003, 2001.

Klein Tank, A. M. G., Wijngaard, J. B., Können, G. P., Böhm, R., Demarée, G., Gocheva, A., Mileta, M., Pashiardis, S., Hejkrlik, L., Kern-Hansen, C., Heino, R., Bessemoulin, P., Müller-Westermeier, G., Tzanakou, M., Szalai, S., Pálsdóttir, T., Fitzgerald, D., Rubin, S., Capaldo, M., Maugeri, M., Leitass, A., Bukantis, A., Aberfeld, R., van Engelen, A. F. V., Forland, E., Mietus, M., Coelho, F., Mares, C., Razuvaev, V., Nieplova, E., Cegnar, T., Antonio López, J., Dahlström, B., Moberg, A., Kirchhofer, W., Ceylan, A., Pachaliuk, O., Alexander, L. V., and Petrovic, P.: Daily dataset of 20th-century surface air temperature and precipitation series for the European Climate Assessment: EUROPEAN TEMPERATURE AND PRECIPITATION SERIES, International Journal of Climatology, 22, 1441–1453, https://doi.org/10.1002/joc.773, http://doi.wiley.com/10.1002/joc.773, 2002.

Lorenz, E. N.: Atmospheric Predictability as Revealed by Naturally Occurring Analogues, J. Atmos. Sci., 26, 636–646, 1969.

Mastrantonas, N., Herrera-Lormendez, P., Magnusson, L., Pappenberger, F., and Matschullat, J.: Extreme precipitation events in the Mediterranean: Spatiotemporal characteristics and connection to large-scale atmospheric flow patterns, International Journal of Climatology, 41, 2710–2728, https://doi.org/10.1002/joc.6985, https://onlinelibrary.wiley.com/doi/10.1002/joc.6985, 2021.

Michelangeli, P., Vautard, R., and Legras, B.: Weather regimes: Recurrence and quasi-stationarity, J. Atmos. Sci., 52, 1237–1256, 1995.

Palmer, T. N.: Predicting uncertainty in forecasts of weather and climate, Reports on Progress in Physics, 63, 71–116, <GotoISI>://000085479700001, 2000.

Peel, M. C., Finlayson, B. L., and McMahon, T. A.: Updated world map of the Ko¨ppen-Geiger climate classification, Hydrol. Earth Syst. Sci., p. 12, 2007.

Peixoto, J. P. and Oort, A. H.: Physics of climate, American Institute of Physics, New York, 1992.

Platzer, P., Yiou, P., Naveau, P., Filipot, J.-F., Thiébaut, M., and Tandeo, P.: Probability Distributions for Analog-To-Target Distances, Journal of the Atmospheric Sciences, 78, 3317 – 3335, https://doi.org/10.1175/JAS-D-20-0382.1, https://journals.ametsoc.org/view/journals/atsc/78/10/JAS-D-20-0382.1.xml, 2021.

Richardson, C. W.: Stochastic simulation of daily precipitation, temperature, and solar radiation, Water Resources Research, 17, 182–190, https://doi.org/10.1029/WR017i001p00182, http://doi.wiley.com/10.1029/WR017i001p00182, 1981.

Ruelle, D.: Ergodic theory of differentiable dynamical systems, Publications Mathématiques de l'Institut des Hautes Études Scientifiques, 50, 27–58, 1979.

Scaife, A. A., Arribas, A., Blockley, E., Brookshaw, A., Clark, R. T., Dunstone, N., Eade, R., Fereday, D., Folland, C. K., and Gordon, M.: Skillful long-range prediction of European and North American winters, Geophysical Research Letters, 41, 2514–2519, 2014.

Sivillo, J. K., Ahlquist, J. E., and Toth, Z.: An ensemble forecasting primer, Weather and Forecasting, 12, 809–818, <GotoISI>://000071577700008, 1997.

Todorovic, P. and Woolhiser, D. A.: A stochastic model of n-day precipitation, Journal of Applied Meteorology, 14, 17–24, 1975.

Toth, Z.: Intercomparison of Circulation Similarity Measures, Mon. Wea. Rev., 119, 55–64, <GotoISI>://A1991FA68200003, 1991.

Toth, Z. and Kalnay, E.: Ensemble forecasting at NCEP and the breeding method, MONTHLY WEATHER REVIEW, 125, 3297–3319, <GotoISI>://A1997YJ55500014, 1997.

Türkes, M., Sümer, U., and Kiliç, G.: Persistence and periodicity in the precipitation series of Turkey and associations with 500 hPa geopotential heights, Climate Research, 21, 59–81, https://doi.org/10.3354/cr021059, http://www.int-res.com/abstracts/cr/v21/n1/p59-81/, 2002.

van den Dool, H. M.: Empirical Methods in Short-Term Climate Prediction, Oxford University Press, Oxford, 2007.

van der Wiel, K., Bloomfield, H. C., Lee, R. W., Stoop, L. P., Blackport, R., Screen, J. A., and Selten, F. M.: The influence of weather regimes on European renewable energy production and demand, Environmental Research Letters, 14, 094 010, https://doi.org/10.1088/1748-9326/ab38d3, https://iopscience.iop.org/article/10.1088/1748-9326/ab38d3, 2019.

Vitart, F., Ardilouze, C., Bonet, A., Brookshaw, A., Chen, M., Codorean, C., Déqué, M., Ferranti, L., Fucile, E., Fuentes, M., Hendon, H., Hodgson, J., Kang, H.-S., Kumar, A., Lin, H., Liu, G., Liu, X., Malguzzi, P., Mallas, I., Manoussakis, M., Mastrangelo, D., MacLachlan, C., McLean, P., Minami, A., Mladek, R., Nakazawa, T., Najm, S., Nie, Y., Rixen, M., Robertson, A. W., Ruti, P., Sun, C., Takaya, Y., Tolstykh, M., Venuti, F., Waliser, D., Woolnough, S., Wu, T., Won, D.-J., Xiao, H., Zaripov, R., and Zhang, L.: The Subseasonal to Seasonal (S2S) Prediction Project Database, Bulletin of the American Meteorological Society, 98, 163–173, https://doi.org/10.1175/BAMS-D-16-0017.1, https://journals.ametsoc.org/doi/10.1175/BAMS-D-16-0017.1, 2017.

von Storch, H. and Zwiers, F. W.: Statistical Analysis in Climate Research, Cambridge University Press, Cambridge, 2001.

Xoplaki, E., Luterbacher, J., Burkard, R., Patrikas, I., and Maheras, P.: Connection between the large-scale 500 hPa geopotential height fields and precipitation over Greece during wintertime, Climate Research, 14, 129–146, https://doi.org/10.3354/cr014129, http://www.int-res.com/abstracts/cr/v14/n2/p129-146/, 2000.

Yiou, P. and Déandréis, C.: Stochastic ensemble climate forecast with an analogue model, Geoscientific Model Development, 12, 723–734, https://doi.org/10.5194/gmd-12-723-2019, https://www.geosci-model-dev.net/12/723/2019/, 2019.

Yiou, P., Goubanova, K., Li, Z. X., and Nogaj, M.: Weather regime dependence of extreme value statistics for summer temperature and precipitation, Nonlinear Processes in Geophysics, 15, 365–378, 2008.

Yiou, P., Salameh, T., Drobinski, P., Menut, L., Vautard, R., and Vrac, M.: Ensemble reconstruction of the atmospheric column from surface pressure using analogues, Climate Dynamics, 41, 1333–1344, https://doi.org/10.1007/s00382-012-1626-3, http://link.springer.com/10.1007/s00382-012-1626-3, 2013.

Zamo, M. and Naveau, P.: Estimation of the Continuous Ranked Probability Score with Limited Information and Applications to Ensemble Weather Forecasts, Mathematical Geosciences, 50, 209–234, 2018.